Oriented Immobilization of Antibody Fragments on Ni-Decorated Single-Walled Carbon Nanotube Devices

Young-Seop Lo,[†,‡,⊥] Dong Hyun Nam,[§,⊥] Hye-Mi So,[†] Hyunju Chang,[†] Ju-Jin Kim,[‡] Yong Hwan Kim,[§,*] and Jeong-O Lee[†,*]

[†]NanoBio Fusion Research Center, Korea Research Institute of Chemical Technology, Daejeon 305-343, Korea, [‡]Department of Physics, Chonbuk National University, Jeonju 561-756, Korea, and [§]Department of Chemical Engineering, Kwangwoon University, Seoul 139-701, Korea. [⊥]These authors contributed equally to this work.

ABSTRACT We herein demonstrate that Ni-decorated single-walled carbon nanotube field effect transistors (SWNT-FETs) combined with antibody fragments can be used as effective biosensing platforms. Nanoscales Ni particles 20 to 60 nm in diameter were formed on the sidewalls of SWNT-FETs using an electrochemical method. Carcinoembryonic antigen (CEA)-binding single chain variable fragments (scFvs) with a hexahistidine tag [$(his)_6$] were synthesized using genetic engineering, and ordered immobilization of anti-CEA ScFvs on Ni nanoparticles was achieved by exploiting the specific interaction between hexahistidine and Ni. Whereas randomly oriented anti-CEA scFvs did not impart a noticeable change of conductance upon addition of CEA, a clear increase in conductance was observed using Ni-decorated SWNT-FETs functionalized with engineered scFvs.

KEYWORDS: scFv · Ni nanoparticle · single-walled carbon nanotube field effect transistor · hexahistidine

Electronic sensors based on single-walled carbon nanotube field effect transistors (SWNT-FETs) are useful for detection of both general molecular and biomolecular adsorption.[1−4] Although some FET sensors employ Schottky contact electrodes as active sensing areas,[5,6] most nanotube or nanowire sensors use intrinsic channels for this purpose. For selective detection of biomolecular analytes, target-specific recognition elements such as antibodies,[7] aptamers,[8] or molecular imprinted polymers (MIPs)[9] are immobilized on the sidewalls of SWNTs or nanowires. In the case of silicon nanowires, silane groups on nanowire surfaces[7] or Si surfaces can be directly used to link recognition elements.[10] With SWNTs, either noncovalent binding linkers such as pyrene-based molecules[11] or alkyl chains may be employed,[12] or carboxyl groups produced after acid treatment can be used to attach recognition elements.[13] In all cases, linkers are designed so that one arm binds to the sensor surface and the other reacts with recognition elements. In most instances, recognition element-binding sites are *N*-hydroxysuccinimide (NHS) or aldehyde groups, which can react with primary amines provided in biomolecules by lysine residues. Unlike synthetic recognition elements, most antibodies contain multiple lysine residues, some of which are located in the antigen-binding variable regions. Therefore, antibody immobilization using lysine-binding linkers results in randomly oriented recognition elements; this lack of structure may reduce the amplitude of the signal emitted after antigen binding. This can be a serious problem with one-dimensional nanostructures, because the total number of recognition elements that can be immobilized on nanostructures is already restricted.

In this report, we show that single-chain variable fragment (scFv) antibodies genetically modified with a hexahistidine tag [$(his)_6$] can be immobilized onto Ni nanoparticles decorating the sidewalls of SWNT-FETs, and that the change of conductance upon target binding was much greater than that seen after random immobilization of scFvs.

RESULTS AND DISCUSSION

Scheme 1 shows our experimental design. While Scheme 1a,b demonstrates SWNT sensors containing randomly oriented whole antibodies and scFvs, respectively. The scFvs are immobilized with all antigen-binding sites fully accessible on the Ni nanoparticles of Scheme 1c. Red spheres in Scheme 1 mark antigen binding moieties in antibodies or scFv.

Carcinoembryonic antigen (CEA), a well-known tumor marker,[14] was used as a model target. Sera from patients with colorectal, gastric, pancreatic, lung, and breast carcinoma, and from patients with medullary thyroid carcinoma, had levels of

*Address correspondence to jolee@krict.re.kr, metalkim@kw.ac.kr.

Received for review May 25, 2009 and accepted September 24, 2009.

Published online October 1, 2009.
10.1021/nn900540a CCC: $40.75

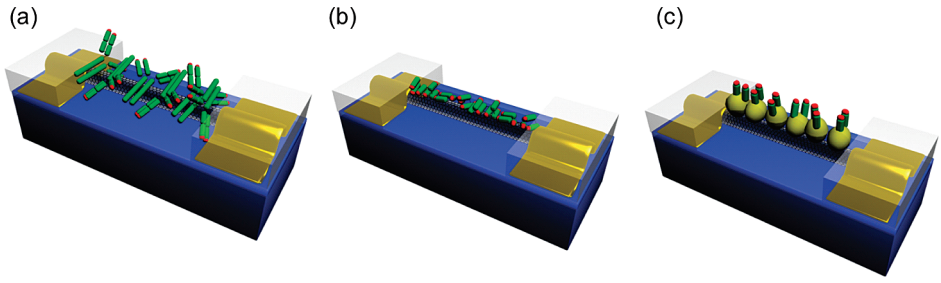

Scheme 1. Schematic diagram of the experimental system: (a) diagram of a SWNT-FET with bound randomly-oriented whole antibody; (b) diagram of a SWNT-FET with randomly-oriented scFv; (c) diagram of a Ni-decorated SWNT-FET with bound scFv.

CEA greater than seen in healthy individuals. CEA is normally detected by immunochemistry, using specific antibodies. In the present report, genetically engineered CEA antibody fragments (scFvs) were employed, because a small recognition element can be of great benefit in construction of sensors of the FET type.[15] Recently, So and colleagues[8] and Kim and co-workers[16] demonstrated the advantages of using smaller recognition elements (aptamers and antibody fragments, respectively) in SWNT-FETs. Further, it is possible to insert a biomolecular "glue", such as a hexahistidine [$(his)_6$] tag, into antibody fragments using genetic engineering.

Anti-CEA scFv recombinant antibodies with $(his)_6$ tag were genetically produced and purified according to the protocol described in Methods section. SWNTs were grown on the Si/SiO_2 substrate by chemical vapor deposition technique and fabricated into devices using photolithography. The detailed device fabrication process is described in the Methods section as well. For immobilization of $(his)_6$-tagged scFvs, we decorated Ni nanoparticles on sidewalls of SWNTs using electrochemical technique.[17,18] Briefly, SWNT-FETs were first insulated using a SiO_x layer, and chronoamperometry, in a probe station, was performed using a standard electrochemical system (2 mM $NiSO_4$ solution with 100 mM KCl as supporting electrolyte) for defined periods of time. Insulation of electrodes is necessary in order to have selective decoration of metal nanoparticles on SWNTs. The source and drain electrodes of the SWNT-FET were used as working electrodes, Pt wire served as a counter-electrode, and Ag/AgCl was the reference electrode. The size and density of Ni nanoparticles can be tuned by variation of the Ni ion concentration in solution, pulse height, and time. We obtained closely packed Ni nanoparticles, of uniform diameter 15−30 nm, by applying 0.4−1 V for 5 s. Figure 1 shows an AFM image of a Ni-decorated SWNT-FET and $I-V_g$ measurement taken before and after the Ni decoration. The effect of Ni decoration on electronic transport characteristics of SWNT-FETs depends heavily on particle sizes and spacing. As shown in Figure 1a, when we have densely packed, smaller (<30 nm) nanoparticles, a decrease of on-current and almost metallic behavior has been observed from Ni-decorated SWNT-FET. When particle sizes are larger than ~30 nm and they are far apart from each other, a positive shift of gate voltages are observed upon Ni decoration. We presume that while smaller Ni nanoparticles instantly oxidized to NiO_x, which has a work function similar to that of SWNTs (4.8 eV),[19] larger nanoparticles maintain their original work function (~5.3 eV).[20]

ScFvs were immobilized on Ni-decorated SWNT-FETs for 6 h in a humidified chamber. After incubation, the transistors were washed with generous amounts of buffer, followed by DI water, and dried in a moisture-free N_2 gas stream prior to further reaction and characterization. Normally, the $(his)_6$ tag binds well to Ni^{2+} ions; we initially confirmed that the tag also bound efficiently to electrochemically grown Ni nanoparticles.

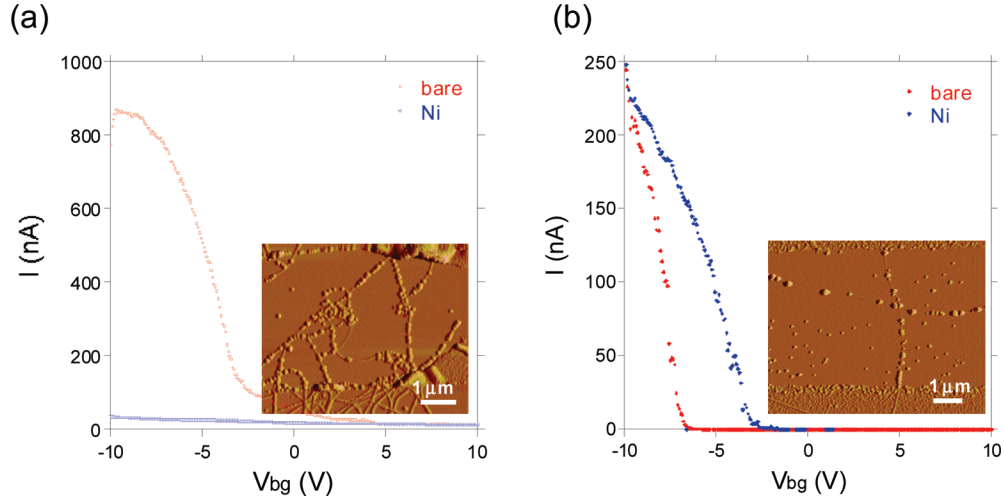

Figure 1. AFM images of Ni-decorated SWNT-FETs and $I-V_g$ characteristics before and after the Ni decoration.

Figure 2 shows atomic force microscopy (AFM) images, and a laser confocal micrograph of an Ni-decorated SWNT-FET, after incubation with $(his)_6$-tagged green fluorescent protein (GFP). The diameter of the Ni nanoparticles was about 20−60 nm in this specific sample. Recently, Park and colleagues reported the oriented immobilization of $(his)_6$-tagged virus particles on Ni nanohairs grown by an electrochemical technique, using an alumina template.[21]

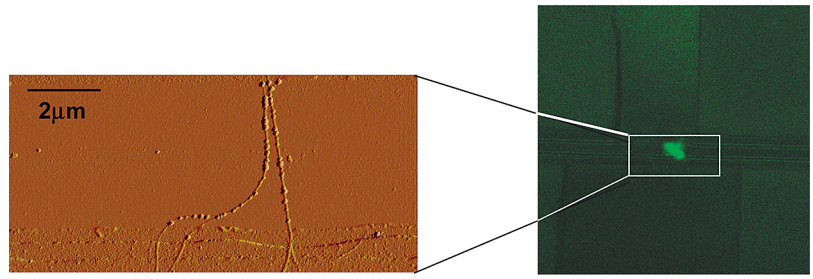

Figure 2. AFM image and confocal micrograph of an Ni-decorated SWNT-FET. The Ni nanoparticles are about 20−60 nm in diameter, and $(his)_6$-tagged GFP is immobilized onto the device.

Detection of CEA using anti-CEA scFv immobilized on Ni-decorated SWNT-FETs was performed as follows. First, 3 μL of buffer solution (100 μM phosphate buffered saline; PBS) was added to an FET and conductance was measured using the Ag/AgCl reference electrode as a liquid gate. When conductance became stabilized, a target solution of known CEA concentration was added to the FET and conductance was monitored in real time. After reaction, each device was washed with an ample amount of DI water and blown dry, and the $I-V_g$ characteristics were measured using Si as a backgate. Figure 3 panels a and b show the real-time conductance measurement and the $I-V_g$ data, respectively. As shown therein, an increase in conductance was observed, in real time, upon introduction of CEA solution, and here we applied 100 mV bias and −100 mV liquid gate voltages (Ag/AgCl). Conductance measured from the devices tends to saturate upon 10−100 ng/mL CEA depending on the device characteristics (Supporting InformationFigure S1). Inset of Figure 3a shows an AFM image of the device after Ni decoration. The increase of conductance observed cannot be explained with electrostatic gating effect, since metal nanoparticles (Ni) sandwiched between the SWNT and target may screen extra charges from the interaction. Rather, we explain this with the change of metal work function, as in the case of Au-decorated SWNT-FET sensors. However, change of conductance due to the change of capacitance should be taken into account as well, since SWNT surfaces are fully packed with Ni nanoparticles and therefore with receptor molecules.[22] $I-V_g$ measurements taken after the reaction also show an increase of conductance whether we use liquid gate or back gate measurement after drying the samples. Figure 3b shows the evolution of $I-V_g$ characteristics (back gate) upon reaction, and the inset of Figure 3b shows liquid gate characteristics. We measured more than 20 Ni-decorated, scFv functionalized SWNT-FETs, and all of them showed increased conductance of 50−100% after the reaction with CEA (Supporting InformationFigure S2). By comparison, SWNT-FET sensors with randomly oriented whole antibodies showed a maximum of 20% change in conductance with 100 ng/mL CEA.[23] The reason for such increase in conductance upon reaction is not fully clear, but CEA is a linear, large molecule of ~240 kDa,[24] and, as scFv molecules immobilized on Ni nanoparticles were closely packed, a sensitivity greater than that afforded by use of whole antibodies may be expected. Also, the surface area of Ni-decorated SWNTs is about 30-fold greater than that of bare SWNTs.[25] Increasing the sensor sur-

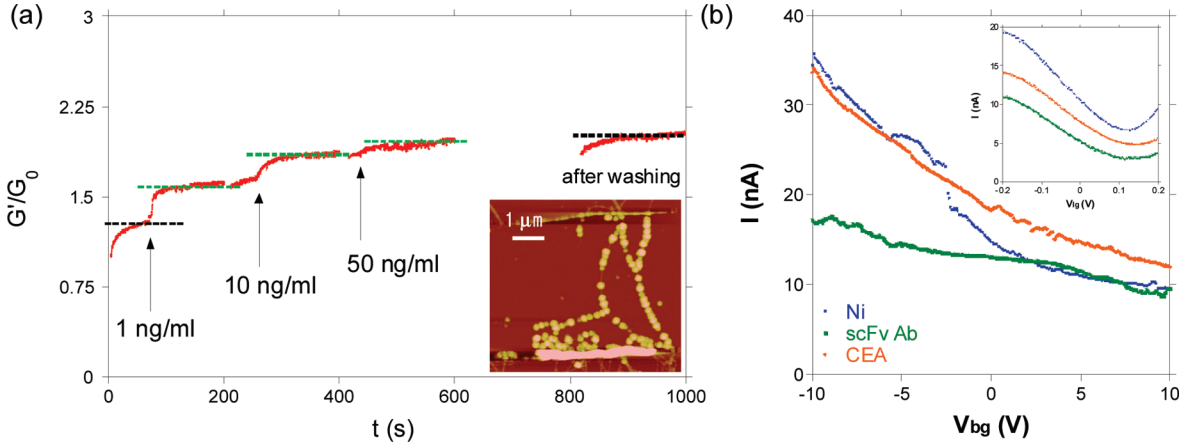

Figure 3. Real-time conductance, and evolution of $I-V_g$ characteristics, in Ni-decorated, scFv-functionalized SWNT-FETs. (a) Real-time conductance. (b) Evolution of $I-V_g$ characteristics throughout detector−ligand interaction. The blue curve shows data after Ni decoration, the green curve shows measurements after addition of scFv, and the orange curve is the $I-V_g$ data obtained after reaction with CEA. The bias voltage was 100 mV. Inset shows the liquid gate measurement from the same device.

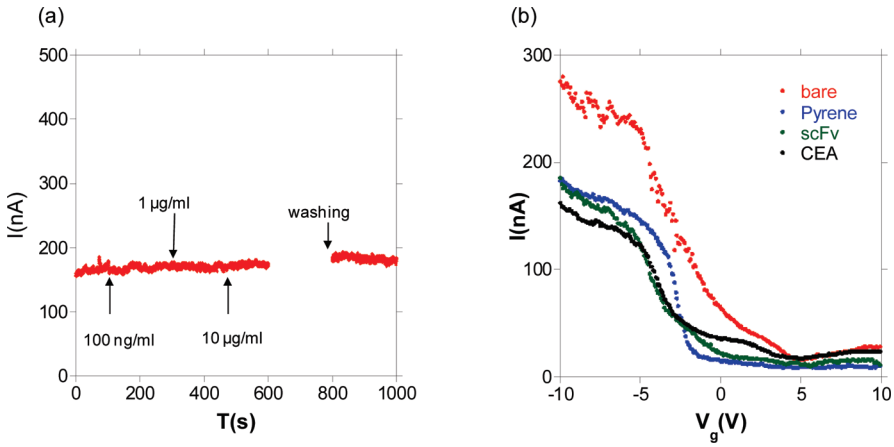

Figure 4. Real-time conductance, and evolution of $I-V_g$ characteristics, in SWNT-FETs carrying randomly oriented scFvs. (a) Real-time conductance. Almost no conductance change was observed after introduction of CEA. (b) Evolution of $I-V_g$ characteristics throughout detector–ligand interaction. The red curve shows measurements from the bare SWNT-FET, the blue curve shows data after pyrene addition, the green curve shows measurements after addition of scFv, and the black curve is the $I-V_g$ data obtained after reaction with CEA. Again, the bias voltage was 100 mV.

face area is valuable in improving sensitivity and reducing detection time.[26]

To explore the effectiveness of oriented immobilization using the $(his)_6$ tag, we immobilized anti-CEA scFv antibodies employing 1-pyrene-*N*-hydroxysuccinimide ester (pyrene). For such immobilization, a device was immersed in 6 mM pyrene in dimethylformamide (DMF) solution for 2 h, washed with clean DMF, and further washed with DI water for 1 h to prevent nonspecific adsorption. Immobilization of anti-CEA scFv then proceeded as described above for Ni-decorated SWNT-FETs. Figure 4 shows electrical characteristics of the reaction with CEA using randomly oriented anti-CEA scFv molecules. As shown by the real-time conductance measurement of Figure 4a, almost no change of conductance was seen even with high concentrations (10 μg/mL) of CEA. In addition, the $I-V_g$ characteristics after reaction also did not alter (Figure 4b). Supporting Information Figure S3 shows $I-V_g$ characteristics of devices with randomly oriented antibody fragments after reaction with CEA. In an effort to understand why randomly oriented anti-CEA scFv antibodies failed to generate signal, we examined the protein structure of anti-CEA scFv, and Figure 5 shows details obtained from crystallographic studies. Ten lysine resides are marked with arrows, and red color indicates the complementarity determining regions (CDRs; these are short amino acid sequences providing the receptor with specificity for any particular antigen) of the heavy chain, and blue color is used to depict the CDR regions of the light chain.

The crystal structure of a ligand-free anti-CEA scFv antibody termed MFE-23 has been determined by Boehm and colleagues.[27] The antigen-binding site of an immunoglobulin includes six hypervariable regions, three from the V_L domains (L1, L2, L3) and the other three from V_H domains (H1, H2, H3).[28] In randomly oriented immobilization of anti-CEA scFv using pyrene, lysine groups on the surface of anti-CEA scFv will be employed for immobilization. MFE-23 contains 10 candidate lysines shown in Figure 5 able to conjugate with succinimidyl ester.[29] Among these, four residues participate in hydrogen bonding that plays an important role in antibody function, and two participate in cation–π interactions that ensure stability of the β-sheet. Therefore, even though these residues are exposed to solvent, they cannot participate in linker conjugation

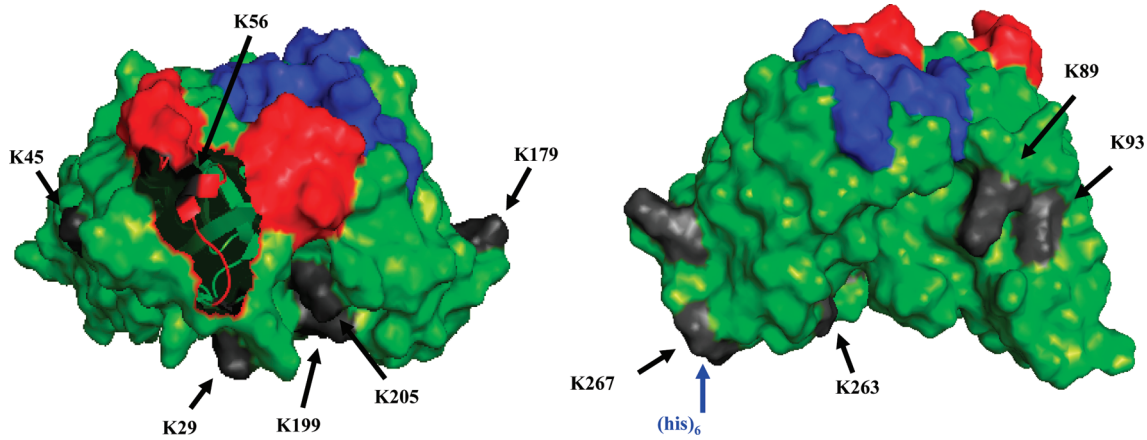

Figure 5. Protein structures of anti-CEA scFv (MFE-23, PDB ID; 1QOK), showing lysine residues and the $(his)_6$ tag at the C-terminus of the protein. Red color indicates the complementarity determining regions (CDRs; these are short amino acid sequences providing the receptor with specificity for any particular antigen) of the heavy chain, and blue color is used to depict the CDR regions of the light chain. The hexahistidine tag was tethered at the C-terminus of the anti-CEA scFv, next to the K267 lysine residue. H1 loop structure is shown in a cartoon model while others are depicted using surface model.

events with maintenance of antibody structural stability. The interactions of these residues are summarized in Table 1.[30]

The remaining four lysines may become covalently bonded to succinimidyl ester. However, if the linker conjugates with K56 or K29, which are located near the H1 loop (shown in a cartoon model in Figure 5), the antigen binding region will be directed toward the surface of the SWNT. The K263 residue is also excluded, because it is too deeply located to be immobilized with succinimidyl ester. The last lysine residue, K179, is fully exposed; the amine group of the side chain can thus react with the linker. Therefore, the probability of CEA detection using randomly oriented anti-CEA scFv is only 10%, whereas immobilization using $(his)_6$ ensures that the binding pocket is fully exposed to CEA. In short, random immobilization of antibody fragments using nonspecific linkage can hamper the detection of target antigen.

On the other hand, signal changes have been observed from sensors with randomly oriented whole antibodies.[23] Scheme 2 compares the structures of a whole antibody (immunoglobulin) and a scFv fragment. A scFv is a fusion of variable regions of the heavy and light chains of immunoglobulin. A scFv retains the specificity of the original antibody, and Fc region of immunoglobulin is omitted in scFv. In the case of whole anti-CEA antibody, it contains multiple lysine resides in the Fc regions, which can be used to react with succinimidyl ester groups on SWNTs. The structure of the Fc region of anti-CEA is unknown, because the three-dimensional (3D) structure of an intact anti-CEA monoclonal antibody has not been reported. However, it is well-known that the constant regions of most antibodies show not only structural similarity but also sequence identity of over 30−40%; the positions of the lysine residues in the Fc region of IgG2a monoclonal antibody (PDB ID: 1IGT), for which a 3D structure is available, have been analyzed. About half of the lysine residues in Fc regions are exposed to the solvent environment and are devoid of any specific interaction; therefore, lysine residues in the Fc region can be reacted with succinimidyl ester on SWNTs to immobilize the antibody and to produce the signal upon antigen binding.

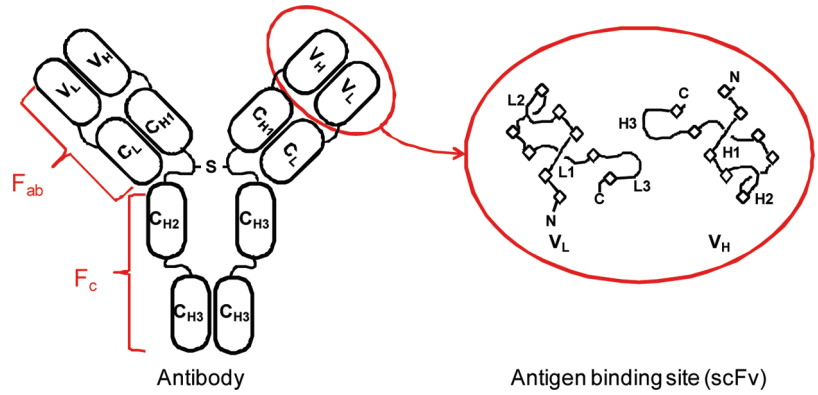

Scheme 2. Schematic diagram of an antibody showing the antigen-binding site.

TABLE 1. List of Lysine Residues in anti-CEA scFv That Participate in Either Hydrogen Bonding or Cation-π Interactions

residues	type of interaction
K267−E178	hydrogen bonding
K89−E72	hydrogen bonding
K93−D116	hydrogen bonding
K199−E241	hydrogen bonding
K45−Y106	cation−π interaction
K205−W207	cation−π interaction

In summary, we have shown that Ni-decorated SWNT-FETs can be an effective biosensor platform when used with $(his)_6$-tagged scFv antibodies as molecular recognition elements. Ni nanoparticles electrochemically deposited on the sidewalls of SWNTs functioned as a support for oriented immobilization of the $(his)_6$-tagged scFv antibodies, and, as the surface area of Ni-decorated SWNTs is much larger than that of bare SWNTs, it was possible to immobilize more recognition antibodies using an Ni-decorated device. Whereas an interaction with CEA was reflected in a large increase in conductance by Ni-decorated SWNT-FETs bearing genetically engineered anti-CEA scFv antibodies, no such change was observed when randomly oriented scFv antibodies were employed. Thus, oriented immobilization of antibody fragments is crucial for good sensor performance, and we suggest that Ni-decoration is an effective method for oriented detector immobilization onto SWNT-FET-based biosensors and increases the reactive area.

METHOD

Device Fabrication. SWNTs were grown on a Si/SiO_2 substrate using a patterned chemical vapor deposition (CVD). Liquid catalyst consisting of $Fe(NO_3)_2 \cdot 9H_2O$ and $Mo(acac)_2$ in methanol was dispersed on substrates with patterned poly(methyl methacrylate). After liftoff, SWNT growth was carried out in 900 °C-heated furnace for 10 min with CH_4 or ethanol as a carbon source. Patterns for electrical leads were formed by photolithography, followed by thermal evaporation of Ti and Au. Channel length between source and drain electrode is fixed to 5 μm. For real-time characterization and metal decoration, all electrodes were carefully insulated with SiO_x. Again, patterns for insulation layer were formed by photolithography, and SiO_x was evaporated using thermal evaporation.

Anti-CEA scFv Production. To produce anti-CEA scFv antibodies, an scFv gene fused with the $(his)_6$ tag at the 3′ end was chemically synthesized, with reference to GenBank sequence 2299568, and cloned into the pMD18 vector (Takara, Otsu, Japan). The target gene (the anti-CEA scFv antibody) was amplified from the pMD18 clone by PCR using a primer pair (sense primer: 5′-

gcg**catatg**aaatacctattgcct-3′ and antisense primer: 5′-gcg**gaattc**tcaatgatgatgatgatg-3′; cleavage sites for *Nde*I and *Eco*RI are shown in bold). PCR was performed in a 50 μL reaction mixture (10× *EX Taq* buffer containing 25 mM $MgCl_2$, 2.5 mM dNTP mixture, 5 U of Takara *EX Taq* polymerase, 100 pM of each primer, and the template plasmid gene). A standard PCR protocol was run for 30 cycles (cycling parameters were denaturation at 94 °C for 30 s, annealing at 55 °C for 30 s, and extension at 72 °C for 60 s), and the final extension was carried out at 72 °C for 10 min. The resulting PCR product was digested with *Nde*I and *Eco*RI and inserted into the pColdIV vector, in which expression of the cloned gene is regulated by the *cspA* low temperature-inducible promoter, to obtain efficient functional protein expression. Correct protein folding is better in this system than when a pET construct is employed. The plasmid (termed pColdIV-anti-CEA scFv in this report) was transformed into the expression host *Escherichia coli* BL21 (λDE3) and a positive clone was selected on an LB agar plate containing 50 μg/mL ampicillin. For anti-CEA scFv antibody expression, an overnight culture of cells (10 mL) was inoculated into 250 mL of LB medium containing 50 μg/mL ampicillin, and the cells were grown to $OD_{600} = 0.6-0.9$ at 37 °C. Thereafter, the culture flask was placed on ice for 30 min and the target gene, under the control of the *cspA* promoter, was fully induced by addition of 0.5 mM isopropyl-β-D-thiogalactopyranoside (IPTG) followed by growth at 15 °C for 24 h. Harvested cells were lysed and recombinant antibodies were purified under native conditions using Ni-NTA resin (Qiagen, Valencia, CA), which specifically bound the recombinant protein by interaction of the $(his)_6$ tag at the C terminus with Ni^{2+}. The cell pellet was resuspended in 10 mL of lysis buffer (50 mM NaH_2PO_4, 300 mM NaCl, 10 mM imidazole [pH 8.0]), also containing lysozyme and Benzonase. The resultant suspension was incubated on ice for 30 min with gentle shaking. Cellular debris and insoluble material were removed by centrifuging at 16000*g* for 20 min at 4 °C. The supernatant, containing recombinant protein, was loaded onto a 0.5 mL Fast Start column. The column was twice washed with 4 mL of washing buffer (50 mM NaH_2PO_4, 300 mM NaCl, and 20 mM imidazole [pH 8.0]). The recombinant protein fused with $(his)_6$ was eluted with two sequential 1 mL fractions of elution buffer (50 mM NaH_2PO_4, 300 mM NaCl, and 250 mM imidazole [pH 8.0]). The eluted solution containing soluble protein was analyzed by Western blotting, according to the method of Burnette.[31]

Functionality Check and Purification of scFvs. ELISA plates were coated with CEA protein (BIODESIGN International, Saco, Maine) and residual binding sites in coated wells were blocked with 5% (w/v) no-fat skim milk, in PBS. Dilutions of the protein solution were added to wells and the plate incubated at room temperature for 2 h. After washing with PBS containing 0.05% (v/v) Tween 20, anti$(his)_6$ mouse monoclonal antibody and alkaline phosphatase (AP)-conjugated rabbit antimouse IgG polyclonal antibody (Abcam, Cambridge, UK) were sequentially added (with intermediate washing steps) to the wells; each of the two incubations was at room temperature for 1 h. After final washing, the activity of scFv antibody bound to CEA was detected using *p*-nitrophenyl phosphate (pNPP) as chromogen (data not shown). For application in nanoFET biosensor construction, it was necessary that the protein should be highly purified both from potentially contaminating proteins and excessive imidazole derived from the elution buffer. Anti-His mAb MagBeads (GenScript, Piscataway, NJ) were used to capture the $(his)_6$-tagged recombinant protein, following the manufacturer's protocol. Excellent purification of anti-CEA scFv antibody was verified by sodium dodecyl sulfate-polyacrylamide gel electrophoresis (SDS-PAGE) (data not shown). The concentration of scFv antibody was determined by the Bradford protein method (using a Bio-Rad protein assay kit; Bio-Rad, Hercules, CA) and bovine serum albumin (BSA) as standard.[32] The eluted antibody was stored at 100 μg/mL in 1 M Tris buffer, pH 7.0 for further use.

Acknowledgment. Financial support was obtained from the Korea Research Council for Industrial Science and Technology, and Ministry of Environment as "The Eco-technopia 21 project".

Supporting Information Available: Conductance *vs* log concentration measured from three different devices, $I-V_g$ (backgate) characteristics of scFv immobilized, Ni decorated SWNT-FETs, and $I-V_g$ (backgate) characteristics of SWNT-FETs with randomly oriented scFv. This material is available free of charge *via* the Internet at http://pubs.acs.org.

REFERENCES AND NOTES

1. Robertson, J. Realistic Applications of CNTs. *Mater. Today* **2004**, *7*, 46–52.
2. Trojanowicz, M. Analytical Applications of Carbon Nanotubes: A Review. *Trends Anal. Chem.* **2006**, *25*, 480–489.
3. Cui, Y.; Wei, Q.; Park, H.; Lieber, C. M. Nanowire Nanosensors for Highly Sensitive and Selective Detection of Biological and Chemical Species. *Science* **2001**, *293*, 1289–1292.
4. Kong, J.; Franklin, N. R.; Zhou, C.; Chaplin, M. G.; Peng, S.; Cho, K.; Dai, H. Nanotube Molecular Wires as Chemical Sensors. *Science* **2000**, *287*, 622–625.
5. Chen, R. J.; Choi, H. C.; Bangsaruntip, S.; Yenilmez, E.; Tang, X.; Wang, Q.; Chang, Y. L.; Dai, H. An Investigation of the Mechanisms of Electronic Sensing of Protein Adsorption on Carbon. *J. Am. Chem. Soc.* **2004**, *126*, 1563–1568.
6. Tang, X.; Bangsaruntip, S.; Nakayama, N.; Yenilmez, E.; Chang, Y. I.; Wang, Q. Carbon Nanotube DNA Sensor and Sensing Mechanism. *Nano Lett.* **2006**, *6*, 1632–1636.
7. Zheng, G.; Patolsky, F.; Cui, Y.; Wang, W. U.; Lieber, C. M. Multiplexed Electrical Detection of Cancer Markers with NW Sensors Arrays. *Nat. Biotechnol.* **2005**, *23*, 1294–1301.
8. So, H.-M.; Won, K.; Kim, Y. H.; Kim, B.-K.; Ryu, B. H.; Na, P. S.; Kim, H.; Lee, J.-O. Single-Walled Carbon Nanotube Biosensors Using Aptamers as Molecular Recognition Elements. *J. Am. Chem. Soc.* **2005**, *127*, 11906–11907.
9. Lee, E.; Park, D.-W.; Lee, J.-O.; Kim, D. S.; Lee, B. H.; Kim, B. S. Molecularly Imprinted Polymers Immobilized on Carbon Nanotube. *Colloids Surf., A* **2008**, *313−314*, 202–206.
10. Stern, E.; Klemic, J. F.; Routenberg, D. A.; Wyrembak, P. N.; Turner-Evans, D. B.; Hamilton, A. D.; La Van, D. A.; Fahmy, T. M.; Reed, M. A. Label-free Immunodetection with CMOS-Compatible Semiconducting Nanowires. *Nature* **2007**, *445*, 519–522.
11. Besteman, K.; Lee, J.-O.; Wiertz, F. G. M.; Heering, H. A.; Dekker, C. Enzyme-Coated Carbon Nanotubes as Single Molecule Biosensors. *Nano Lett.* **2003**, *3*, 727–730.
12. Chen, R. J.; Bangsaruntip, S.; Drouvalakis, K. A.; Kam, N. W.; Shim, M.; Li, Y.; Kim, W.; Utz, P. J.; Dai, H. Noncovalent Functionalization of CNT for Highly Specific Electronic Biosensors. *Proc. Natl. Acad. Sci. U.S.A.* **2003**, *100*, 4984–4989.
13. Yu, X.; Kim, S. N.; Papadimitrakopoulos, F.; Rusling, J. F. Protein Immunosensor Using Single-Wall Carbon Nanotube Forests with Electrochemical Detection of Enzyme Labels. *Mol. BioSyst.* **2005**, *1*, 70–78.
14. Sten, Hammarström. The Carcinoembryonic Antigen (CEA) Family: Structures, Suggested Functions, and Expression in Normal and Malignant Tissues. *Semin. Cancer Biol.* **1999**, *9*, 67–81.
15. Lee, J.-O.; So, H.-M.; Jeon, E.-K.; Chang, H.; Won, K.; Kim, Y. H. Aptamer as Molecular Recognition Elements for Electrical Nanobiosensors. *Anal. Bioanal. Chem.* **2008**, *390*, 1023–1032.
16. Kim, J. P.; Lee, B. Y.; Hong, S.; Sim, S. J. Ultrasensitive Carbon Nanotube-Based Biosensors Using Antibody-Binding Fragments. *Anal. Biochem.* **2008**, *381*, 193–198.
17. Quinn, B. M.; Dekker, C.; Lemay, S. G. Electrodeposition of Noble Metal Nanoparticles on Carbon Nanotubes. *J. Am. Chem. Soc.* **2005**, *127*, 6146–6147.
18. Quinn, B. M.; Lemay, S. G. Single-Walled Carbon Nanotubes as Templates and Interconnects for Nanoelectrodes. *Adv. Mater.* **2006**, *18*, 855–859.
19. Sze, S. M.; Ng, K. K. Metal Semiconductor Contacts. In *Physics of Semiconductor Devices,* 3rd ed.; Wiley: New York, 2003; pp 136−137.

20. Yang, C. J.; Park, J. I.; Cho, Y. R. Enhanced Field-Emission Obtained from NiO-Coated Carbon Nanotubes. *Adv. Eng. Mater.* **2007**, *9*, 88–91.
21. Park, J.-S.; Cho, M. K.; Lee, E. J.; Ahn, K.-Y.; Lee, K. E.; Jung, J. H.; Cho, Y.; Han, S.-S.; Kim, Y. K.; Lee, J. A. Highly Sensitive and Selective Diagnostic Assay Based on Virus Nanoparticles. *Nat. Nanotechnol.* **2009**, *4*, 259–264.
22. Heller, I.; Janssens, A. M.; Männik, J.; Minot, E. D.; Lemay, S. G.; Dekker, C. Identifying the Mechanism of Biosensing with Carbon Nanotube Transistors. *Nano Lett.* **2008**, *8*, 591–595.
23. Park, D.-W.; Kim, Y.-H.; Kim, Kim, B. S.; So, H.-M.; Won, K.; Lee, J.-O.; Kong, K.; Chang, H. Detection of Tumor Markers Using Single-Walled Carbon Nanotube Field Effect Transistors. *J. Nanosci. Nanotechnol.* **2006**, *6*, 3499–3502.
24. Boehm, M. K.; Perkins, S. J. Structural Models for Carcinoembryonic Antigen and Its Complex with the Single-Chain Fv Antibody Molecule MFE23. *FEBS Lett.* **2000**, *475*, 11–16.
25. We modeled a bare SWNT as a half cylinder with radius of 2 nm and 5 μm long (surface area $S = \pi rh = 3.14 \times 10^{-14}$ m^2). In the case of Ni-decorated SWNTs, if we consider that 30 nm sized Ni nanoparticles are closely packed on 5 μm SWNTs, we have about 160 nanoparticles. In this case, we calculated surface areas of 160 hemispheres with 30 nm diameter ($S = 2\pi r^2 160 \approx 9 \times 10^{-13}$ m^2).
26. Squires, T. M.; Messinger, R. J.; Manalis, S. R. Making It Stick: Convection, Reaction and Diffusion in Surface-Based Biosensors. *Nat. Biotechnol.* **2008**, *26*, 417–426.
27. Boehm, M. K.; Corper, A. L.; Wan, T.; Sohi, M. K.; Sutton, B. J.; Thornton, J. D.; Keep, P. A.; Chester, K. A.; Begent, R. H.; Perkins, S. J. Crystal Structure of the Anti-(carcinoembryonic antigen) Single-Chain Fv Antibody MFE-23 and a Model for Antigen Binding Based on Intermolecular Contacts. *Biochem. J.* **2000**, *346*, 519–528.
28. Al-Lazikani, B.; Lesk, A. M.; Chothia, C. Standard Conformations for the Canonical Structures of Immunoglobulins. *J. Mol. Biol.* **1997**, *273*, 927–948.
29. Protein data bank, http://www.rcsb.org, PDB ID 1QOK (accessed March 2009).
30. Tina, K. G.; Bhadra, R.; Srinivasan, N. PIC: Protein Interactions Calculator. *Nucleic Acids Res.* **2007**, *35*, 473–476; http://crick.mbu.iisc.ernet.in/~PIC/job.html.
31. Burnette, W. N. "Western Blotting": Electrophoretic Transfer of Proteins from Sodium Dodecyl Sulfate Polyacrylamide Gels to Unmodified Nitrocellulose and Radiographic Detection with Antibody and Radioiodinated Protein A. *Anal. Biochem.* **1981**, *112*, 195–203.
32. Bradford, M. M. A Rapid and Sensitive Method for the Quantitation of Microgram Quantities of Protein Utilizing the Principle of Protein-Dye Binding. *Anal. Biochem.* **1976**, *72*, 248–254.